proceedings

MDPI

Abstract

A simple strategy to reduce the standing wave heat pattern in vibro-thermography based on 2D-FFT

Stefano Laureti [1,*], Masashi Ishikawa [2], Rocco Zito [1], Marco Ricci [1], and Hideo Nishino [2]

[1] DIMES Dept., University of Calabria, 87036, Arcavacata di Rende (CS), Italy;
[2] Graduate School of Technology, Industrial and Social Sciences, Tokushima University, Tokushima, 2-1 Minamijosanjima, Tokushima, 770-8506, Japan;
* Correspondence: stefano.laureti@unical.it ;

Keywords: *active thermography, vibro-thermography, standing wave, pattern removal, image processing*

Abstract – Vibrothermography is an effective non-destructive testing technique for detecting closed defects like cracks and delaminations through frictional heat generated under ultrasonic excitation. However, its accuracy is often reduced by standing wave patterns that create periodic temperature artifacts in non-defective areas, leading to false positives. To overcome this, we propose an image processing approach using 2D Fourier Transform (2D-FFT) to reduce SW-induced patterns in the frequency domain. This enhances defect visibility by suppressing unwanted heat signatures. The method is evaluated on a cracked PMMA plate and a hollow tube of the same material.

1 Introduction

Active thermography (AT) is a widely used nondestructive testing and evaluation method applied in aerospace, automotive [1], civil engineering [2], and cultural heritage monitoring [3], to mention some. AT involves applying a heat stimulus to a sample to break its thermal equilibrium. As heat diffuses, an IR camera records the surface temperature evolution. Defects like cracks or voids appear as regions with abnormal temperature compared to their surroundings [4]. Heat can be delivered by various sources, typically halogen lamps, lasers, flash heads, or LEDs. Alternatively, methods like eddy-current or frictional heating from mechanical vibrations can be used [5]. Ultrasound-excited AT—vibrothermography (VT)—leverages frictional heating at defect sites to detect closed defects such as cracks and delaminations [6,7]. However, VT often suffers from standing waves (SWs) patterns that create periodic temperature artifacts, causing false positives [8]. Existing solutions like frames averaging are often inadequate [9]. We propose an automated image processing method using 2D Fourier Transform (2D-FFT) to isolate and remove SW patterns in the frequency domain, preserving true defect signals. The approach is validated on cracked CFRP and PMMA samples using both qualitative and quantitative metrics.

2.1 Vibro-thermography fundamentals and SWs patter problem

VT operates on two primary principles. First of all, defects within a material have different elastic characteristics compared to the surrounding intact areas. This difference leads to increased acoustic damping, thus greater heat generation in the defective regions. Secondly, defects alter the material's thermal properties, which in turn affects heat flow through the sample. These combined effects make defects to appear as temperature irregularities, which can be detected by monitoring the sample surface temperature via an IR camera. More in detail, when a time varying stress σ_{ac} is applied to a sample, the resulting mechanical vibrations get damped during their propagation and the loss is converted into heat. This conversion S is the result of two effects, namely the thermoelastic and

Citation: To be added by editorial staff during production.

Academic Editor: Firstname Lastname

Published: date

hysteresis (or loss angle), $S = K_t\sigma_{ac} + K_l\sigma_{ac}^2$, with K_t and K_l being complex constants denoting the thermoelastic and hysteresis effects, respectively. In general, a good thermal signal can be obtained from polymers as they provide high acoustical damping. In addition, the thermal conductivity of such materials is relatively low, so that acoustic energy dissipated at defects sites remain localized, aiding in turns for their detection – frictional rubbing between contacting asperities is a good example of such localization effect [6].

However, considering the ultrasonic excitation frequency range employed usually in VT, the size and thickness of the tested specimens, as well as their shape, standing waves (SWs) might be triggered and established, which results in undesired heat spots at locations corresponding to the SWs antinodes. As a results, the faithful detection of potential defects can be hindered by such heat patterns, especially when their thermal fingerprints are similar, or when these are superimposed, an example being showed in Figure 1:

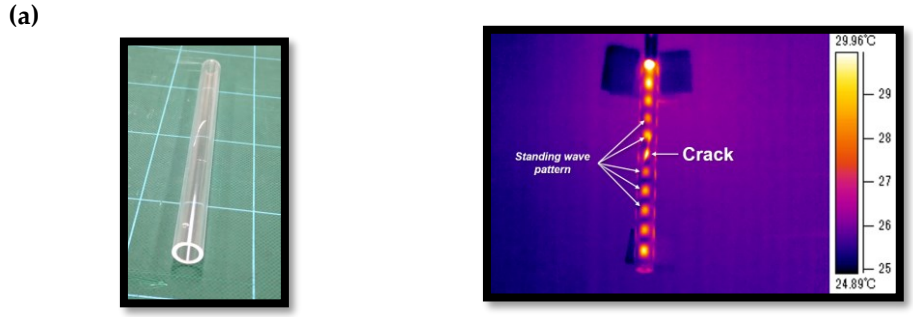

Figure 1: (a) a picture of a cracked PMMA hollow cylinder; (b) thermogram obtained from VT inspection. The detection of the crack is partially hindered by the SW heat pattern.

3 Proposed algorithm

The pivot of the proposed algorithm is that SW-induced heat patterns manifest, in general, as relatively low-frequency modulations in the thermograms, in contrast to the typically higher-frequency components associated with defect-induced thermal signatures. Moreover, they are often oriented along a distinct spatial direction. Thus, they can be separated – filtered - from each other if their thermal signatures are compared in the wavevector domain using the 2D Fast Fourier Transform $\mathcal{F}\{\cdot\}$. To further aid this comparison, a spatial domain detrending is implemented as a pre-processing step using a polynomial surface fitting.

3.1 Pre-processing: polynomial surface fitting for detrending

The thermograms are a series of IR images captured at different time instants $D(x, y, t)$. To remove low-frequency spatial trends, which are mainly due to inhomogeneous heating across the sample, a 2D polynomial surface of degree $n = 3$ is fitted to each frame t. To do so, a set of minima along each row x_k are extracted:

$$z_k = \min D(x_k, :, t) \tag{1}$$

Then, a polynomial basis of is constructed, such that:

$$\Phi(x, y, t) = \sum_{i=0}^{3}\sum_{j=0}^{3-i} c_{ij}^{(t)} x^{i^{(t)}} y^{j^{(t)}} \tag{2}$$

with coefficients $c_{ij}^{(t)}$ by solving the normal equations in the least-square sense:

$$\boldsymbol{A}^{(t)}\boldsymbol{c}^{(t)} = \boldsymbol{z}^{(t)} \tag{3}$$

with $\boldsymbol{A}$ the model matrix constructed from the spatial coordinates (x_i, y_i) of the detected minima and a corresponding observation vector $\boldsymbol{z}^{(t)}$containing their intensity values, see Eq.(1). The detrended data $D_d(x, y, t)$ is then obtained as:

$$D_d(x,y,t) = D(x,y,t) - \Phi(x,y,t) \quad (4)$$

3.2 Frequency-domain analysis and adaptive masking

A specific frame captured at time t_0 is here considered, i.e. $D_d(x,y,t_0)$, being one frame at which a given defect is highly visible. Two regions of interests (ROIs) are then manually selected, i.e. a background ROI (ROI_{bg}) that is a pixels area showing SWs heating pattern, and one on the defect (ROI_{sig}). Both ROIs are then zero-padded before computing their 2D-FFTs up to the pixels dimensions of the full frame, $F_{bg}(u,v)$ and $F_{sig}(u,v)$, with u and v being the spatial frequency coordinate. To identify how the spectral energy is distributed radially, $\rho(r)$ is computed from $|F_{bg}(u,v)|$ as:

$$\rho(r) = \frac{1}{N_r} \sum_{(u,v)\ s.t.\ R[u,v]=r} |F_{bg}(u,v)| \quad (5)$$

with $R(u,v) = \sqrt{(u-u_o)^2 + (v-v_o)^2}$, with (u_o, v_o) denoting the center coordinates of the frequency domain. Then, the maximum of $\rho(r)$ is identified, i.e. where the signal energy peaks – and an annular region of a arbitrary width is defined around it with an inner radius r_{in} and outer radius r_{out}. This initial annular mask is then adapted to spot the differences between the two ROIs by computing $\Delta F(u,v) = |F_{sig}(u,v)| - |F_{bg}(u,v)|$ and obtaining the refined binary mask suppression $M(u,v)$ as:

$$M(u,v) = \begin{cases} 0, & if\ \Delta F(u,v) < T\ and\ r_{in} \le R(u,v) \le r_{out} \\ 1, & otherwise \end{cases} \quad (6)$$

with T being a percentile threshold arbitrarily set to 70%. Additionally, a morphological dilation can be applied to $M(u,v)$ to ensure a comprehensive suppression of SWs, especially when the pattern is not spatially aligned with the defect signature. Finally, the filtered frames $D_f(x,y,t)$ are obtained by $\mathcal{F}^{-1}\{D_d(u,v,t) \cdot M(u,v)\}$.

4 Results and conclusions

The experimental setup comprises an ultrasonic welder (HW-D250H-28, Nippon Avionics Co., Ltd.), with an ultrasonic horn attached to the specimen surface, exciting it with a 28-kHz ultrasound wave. The surface temperature distribution during the vibration was recorded using an infrared camera (A315, FLIR). Two samples have been inspected, i.e. the PMMA cylinder shown in Figure 1 and a cracked PMMA plate, see [9]. The qualitative results of the algorithm are shown in Figure 2, while the Signal-to-noise ration have been also computed as $SNR = |mean(ROI_{sig}) - mean(ROI_{bg})|/std(ROI_{bg})$ and shown in Table 1.

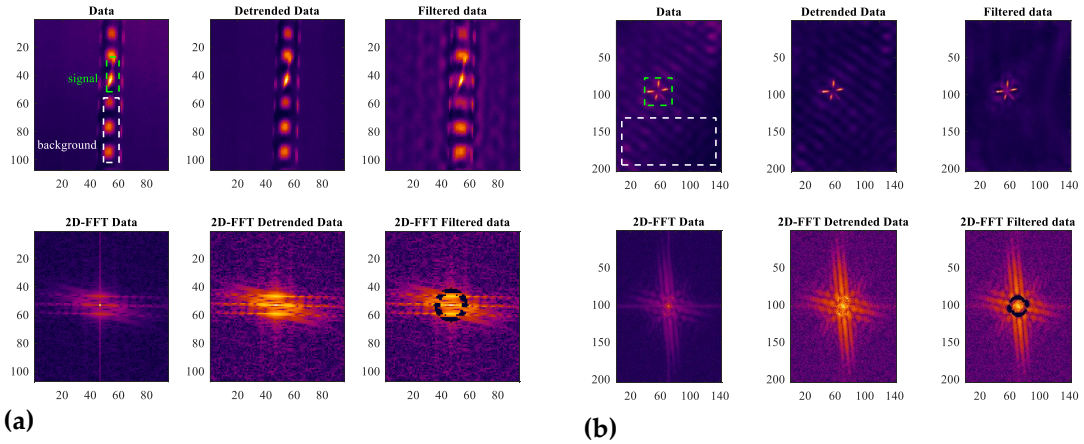

Figure 2: (a) a series of thermograms (top row) showing the steps of the filtering algorithms, the selected pixel areas, and the obtained results for the PMMA hollow cylinder, together with the corresponding 2D-FFTs; (b) same as (a), but for the PMMA plate.

Table 1. SNRs values

	Data	Detrended Data	Filtered Data
Hollow cylinder	0.48	0.20	0.13
Plate	2.40	2.86	4.80

It can be concluded that the suppression mask (black circular masks) enhances the defect detection making the whole length of the crack visible for the cylinder specimen, while for the plate specimen leads to a dramatic reduction of the standing wave pattern. It should be noted that removing the SWs pattern is more difficult for the cylinder specimen than for the plate specimen – the crack signature is on top of the heat pattern, connecting two of the heat spots - this can be appreciated in the computed SNRs.

Author Contributions: Conceptualization, **S.L.** and **M.I**.; methodology, **M.I.**, **H.N**, **S.L.**, **M.R**. and **R.Z**.; software, **S.L**. and **R.Z**; validation, **M.I.**, **H.N**, **S.L.**, **M.R**. and **R.Z**.; investigation **S.L.** and **M.I**; data curation, **S.L**.; writing—original draft preparation, **S.L**.; writing—review and editing, **M.I.**, **H.N**, **S.L.**, **M.R**. and **R.Z**.; visualization, **S.L.**; All authors have read and agreed to the published version of the manuscript.

Funding: This research was supported by Japan Society for the Promotion of Science (JSPS) KAKENHI Grant Number JP 21K04550.

Institutional Review Board Statement: Not applicable.

Informed Consent Statement: Not applicable.

Data Availability Statement: Data is made available from the Authors upon reasonable request.

Acknowledgments: Stefano Laureti acknowledges the EU funded MSCA-DN-2022-01 "MetacMed" project (GA n°101119738) for financial support (www.metacmed.eu) .

Conflicts of Interest: The authors declare no conflicts of interest.

References

1. Hung, Y. Y., Chen, Y. S., Ng, S. P., Liu, L., Huang, Y. H., Luk, B. L., ... & Chung, P. S. (2009). Review and comparison of shearography and active thermography for nondestructive evaluation. *Materials Science and Engineering: R: Reports*, *64*(5-6), 73-112.
2. Milovanović, B., & Banjad Pečur, I. (2016). Review of active IR thermography for detection and characterization of defects in reinforced concrete. *Journal of Imaging*, *2*(2), 11.
3. Laureti, S., Sfarra, S., Malekmohammadi, H., Burrascano, P., Hutchins, D. A., Senni, L., ... & Ricci, M. (2018). The use of pulse-compression thermography for detecting defects in paintings. *Ndt & E International*, *98*, 147-154.
4. Maldague, X. (2000). Applications of infrared thermography in nondestructive evaluation. *Trends in optical nondestructive testing*, 591-609.
5. Ciampa, F., Mahmoodi, P., Pinto, F., & Meo, M. (2018). Recent advances in active infrared thermography for non-destructive testing of aerospace components. *Sensors*, *18*(2), 609.
6. Rantala, J., Wu, D., & Busse, G. (1996). Amplitude-modulated lock-in vibrothermography for NDE of polymers and composites. *Research in Nondestructive Evaluation*, *7*, 215-228.
7. Renshaw, J., Chen, J. C., Holland, S. D., & Thompson, R. B. (2011). The sources of heat generation in vibrothermography. *Ndt & E International*, *44*(8), 736-739.
8. Ishikawa, M., Maeda, R., Nishino, H., Koyama, M., & Fukui, R. (2025). Waves causing undesired heat pattern detected via ultrasound-excited active thermography. *Infrared Physics & Technology*, *145*, 105652.
9. Takahashi, S., Ishikawa, M., Nishino, H., Koyama, M., & Fukui, R. (2023). An Examination of a Method to Reduce the Effect of Standing-Wave Heat Generation in Ultrasound-Excited Thermography Inspection. *Engineering Proceedings*, *51*(1), 22.